JOURNAL OF COMPUTATIONAL PHYSICS 87, 25–46 (1990)

Multigrid and Defect Correction for the Steady Navier–Stokes Equations*

BARRY KOREN

Centre for Mathematics and Computer Science, P.O. Box 4079, 1009 AB Amsterdam, The Netherlands

Received April 28, 1988; revised April 17, 1989

Theoretical and experimental convergence results are presented for nonlinear multigrid and iterative defect correction applied to finite volume discretizations of the full, steady, 2D, compressible Navier–Stokes equations. Iterative defect correction is introduced for circumventing the difficulty in solving Navier–Stokes equations discretized with a second- or higher-order accurate convective part. By Fourier analysis applied to a model equation, an optimal choice is made for the operator to be inverted in the defect correction iteration. As a smoothing technique for the multigrid method, collective symmetric point Gauss–Seidel relaxation is applied with as the basic solution technique: exact Newton iteration applied to a continuously differentiable, first-order upwind discretization of the full Navier–Stokes equations. For non-smooth flow problems, the convergence results obtained are already competitive with those of well-established Navier–Stokes methods. For smooth flow problems, the present method performs better than any standard method. Here, first-order discretization error accuracy is attained in a single multigrid cycle, and second-order accuracy in only one defect correction cycle. The method contributes to the state of the art in efficiently computing compressible viscous flows.

1. INTRODUCTION

1.1. *Navier–Stokes Equations*

The Navier–Stokes equations considered are:

$$\frac{\partial}{\partial x}\begin{pmatrix} \rho u \\ \rho u^2 + p \\ \rho uv \\ \rho u\left(e + \dfrac{p}{\rho}\right) \end{pmatrix} + \frac{\partial}{\partial y}\begin{pmatrix} \rho v \\ \rho uv \\ \rho v^2 + p \\ \rho v\left(e + \dfrac{p}{\rho}\right) \end{pmatrix}$$

* This work was supported by the European Space Agency (ESA), via Avions Marcel Dassault-Bréguet Aviation (AMD-BA).

0021-9991/90 $3.00

$$-\frac{1}{\mathrm{Re}}\left[\frac{\partial}{\partial x}\begin{pmatrix}0\\ \tau_{xx}\\ \tau_{xy}\\ \tau_{xx}u+\tau_{xy}v+\dfrac{1}{\gamma-1}\dfrac{1}{\mathrm{Pr}}\dfrac{\partial(c^2)}{\partial x}\end{pmatrix}+\frac{\partial}{\partial y}\begin{pmatrix}0\\ \tau_{xy}\\ \tau_{yy}\\ \tau_{yy}v+\tau_{xy}u+\dfrac{1}{\gamma-1}\dfrac{1}{\mathrm{Pr}}\dfrac{\partial(c^2)}{\partial y}\end{pmatrix}\right]=0, \tag{1.1a}$$

with

$$\tau_{xx}=\frac{4}{3}\frac{\partial u}{\partial x}-\frac{2}{3}\frac{\partial v}{\partial y},$$

$$\tau_{xy}=\frac{\partial u}{\partial y}+\frac{\partial v}{\partial x}, \tag{1.1b}$$

$$\tau_{yy}=\frac{4}{3}\frac{\partial v}{\partial y}-\frac{2}{3}\frac{\partial u}{\partial x}.$$

For a detailed description of the various quantities used, assumptions made, and so on, we refer to any standard textbook. Suffice to say here that these are the full Navier–Stokes equations with the main assumptions made: zero bulk viscosity and constant diffusion coefficients. (So, the flow is assumed to be laminar and its diffusion coefficients are assumed to be temperature-independent.)

1.2. *Discretization Method*

The present paper focuses on the solution method, the discretization method being given. For a detailed description of the discretization used, we refer to [8]. In this section, only a summary is given of the discretization characteristics that are relevant for the present paper.

Since we also want to be able to compute Euler flow solutions ($1/\mathrm{Re}=0$) with possibly occurring discontinuities, the Navier–Stokes equations (1.1) are discretized in their integral form. A straightforward and simple discretization of the integral form is obtained by subdividing the computational domain into finite volumes and by requiring that the integral form holds for each finite volume separately. This discretization requires an evaluation of a convective and diffusive flux vector at each finite volume wall.

1.2.1. *Evaluation of Convective Fluxes*

Because of good experiences with the Euler equations [5, 6, 7, 15], for the evaluation of the convective fluxes we prefer an upwind approach. In here, the convective flux vector is assumed to be constant along each cell face, and to be determined by a uniformly constant left and right state only. For the 1D Riemann problem thus obtained, an approximate Riemann solver is applied.

The choice of the left and right state, to be used as entries for the approximate Riemann solver, determines the accuracy of the convective discretization. First-order accuracy is obtained, in the standard way, by taking the left and right state equal to that in the corresponding adjacent volume [5, 6]. Higher-order accuracy is obtained by applying low-degree piecewise polynomial functions, using two or three adjacent volume states for the left and right state separately [7, 15]. The higher-order accurate polynomial function used is Van Leer's κ-function [10]. This function is general in the sense that it contains a variable $\kappa \in [-1, 1]$ that can be used for choosing any higher-order approximation ranging from central ($\kappa = 1$) to fully one-sided upwind ($\kappa = -1$). A survey of some characteristic κ-values and their corresponding properties in the case of Euler flow computations has been given in [7]. As an optimal value for κ in the case of Navier–Stokes flows, we found by error analysis: $\kappa = \frac{1}{3}$, for which value we also constructed a new (monotonicity preserving) limiter [8].

For the approximate Riemann solver, in [8] we consider two possibilities which both have continuous differentiability (a prerequisite for our solution method), namely Osher's [12] and Van Leer's [9] scheme. Theoretical analysis and numerical experiments show that Osher's scheme is to be preferred above Van Leer's scheme for an accurate resolution of shear flows. Therefore, in the present paper, we only apply Osher's scheme.

1.2.2. *Evaluation of Diffusive Fluxes*

For the evaluation of the diffusive fluxes, the central, second-order accurate technique as outlined in [13] is applied. So, for the necessary computation, at each volume wall, of ∇u, ∇v, and ∇c^2, the technique uses, at the inner volume walls, a shifted volume overlying the volume wall considered.

To conclude, the discretization to be considered for the full Navier–Stokes equations can be either first-order accurate (first-order convection plus second-order diffusion), or second-order accurate (second- or third-order convection plus—standard—second-order diffusion).

2. Convergence of Multigrid

The same multigrid method which has been used with success for the first-order discretized Euler equations [5, 6] is taken as a point of departure for both the first- and second-order discretized Navier–Stokes equations. The method makes use of symmetric point Gauss–Seidel relaxation as a smoothing technique. In here, one or

more exact Newton steps are performed for the collective relaxation of the four state vector components in each finite volume. (Usually, the convergence of the Newton iteration is so fast that in a substantial majority of all cells, only a single Newton step is necessary.) For the first-order discretized Euler equations, point Gauss–Seidel relaxation turned out to be a good smoother, thus enabling a good multigrid acceleration. However, in general, for higher-order discretized Euler equations the good smoothing property is lost. The cause of this difference is the fact that the system of first-order discretized equations is always diagonally dominant, whereas the system of higher-order discretized equations is not. Obviously, this difference will also exist for Navier–Stokes flows with high Reynolds number. We do not yet look for some remedy, but first we investigate how smoothing evolves with increasingly dominating convection.

The first and major change that we propose for going from Euler to full Navier–Stokes is to extend both the residual operator and its derivative matrix, with the full diffusive part coming from the Navier–Stokes equations. Notice that the differential operator $(\partial/\partial u, \partial/\partial v, \partial/\partial c, \partial/\partial z)^T$, introduced in [5] as a convenient differential operator for the Euler equations, is also very convenient for the diffusive part of the Navier–Stokes equations. The second change that we propose is to replace the piecewise constant correction prolongation by a bilinear prolongation, thus satisfying the rule that the sum of the order of prolongation and the order of restriction should exceed the order of the differential equation ($m_p + m_r > 2m$) [3].

2.1. *Investigation Method*

To investigate the convergence properties of the multigrid method proposed, both theoretical and experimental convergence results are presented. The theoretical results are obtained by performing a smoothing analysis for a model equation. The experimental results are obtained by considering two standard flow problems; a problem with a smooth solution and a problem with a non-smooth solution. The theoretical analysis and the experimental analysis will be discussed in more detail in the next two sections.

2.1.1. *Smoothing Analysis*

Since Fourier analysis cannot be applied to the full, steady, 2D Navier–Stokes equations, here we can only obtain an indication of the smoothing properties that may be expected. For this purpose, we consider the scalar, linear convection diffusion equation

$$\frac{\partial u}{\partial x} + \frac{\partial u}{\partial y} - \varepsilon\left(\frac{\partial^2 u}{\partial x^2} + \frac{\partial^2 u}{\partial x\,\partial y} + \frac{\partial^2 u}{\partial y^2}\right) = 0, \tag{2.1}$$

for which the relaxation direction and the important weight ε (of the diffusive operator in relation to that of the convective operator) will be varied. The choice of both the convective operator's characteristic direction and the diffusive

operator's eigendirection is arbitrary and fixed. The loss of generality by taking both directions fixed is compensated for by considering the four extreme relaxation directions; the downwind, the upwind, and the two crosswind ones. Rigorous convergence studies are supposed to be possible only by performing numerical experiments with the full Navier–Stokes equations. Yet, pronounced (negative) results obtained by Fourier analysis will be taken sufficiently decisive to refrain from such experiments.

For the integral form of (2.1), for each finite volume $\Omega_{j,k}$, $j = 1, 2, ..., J$, $k = 1, 2, ..., K$, we use

$$\oint_{\partial\Omega_{j,k}} (un_x + un_y)\, ds - \varepsilon \oint_{\partial\Omega_{j,k}} \left(\frac{\partial u}{\partial x} n_x + \frac{\partial u}{\partial x} n_y + \frac{\partial u}{\partial y} n_y \right) ds = 0, \qquad \forall_{j,k}, \tag{2.2}$$

with $\partial\Omega_{j,k}$ the boundary of $\Omega_{j,k}$. The two parts of the Navier–Stokes discretization to be modelled further, are: (i) the upwind treatment of convection, either first- or higher-order accurate (non-limited $\kappa = \frac{1}{3}$), and (ii) the central second-order accurate treatment of diffusion. Assuming a finite volume grid with cell faces which are equidistant and parallel to the x- and y-axis ($\Delta x = \Delta y = h$, Fig. 2.1), the evaluation of convective flux terms yields

$$\begin{aligned} \oint_{\partial\Omega_{j,k}} un_x\, ds &= (u^l_{j+1/2,k} - u^l_{j-1/2,k})h, \\ \oint_{\partial\Omega_{j,k}} un_y\, ds &= (u^l_{j,k+1/2} - u^l_{j,k-1/2})h, \end{aligned} \tag{2.3a}$$

with

$$\begin{aligned} u^l_{j+1/2,k} &= \alpha_1 u_{j-1,k} + \alpha_2 u_{j,k} + \alpha_3 u_{j+1,k}, \\ u^l_{j,k+1/2} &= \alpha_1 u_{j,k-1} + \alpha_2 u_{j,k} + \alpha_3 u_{j,k+1}, \end{aligned} \tag{2.3b}$$

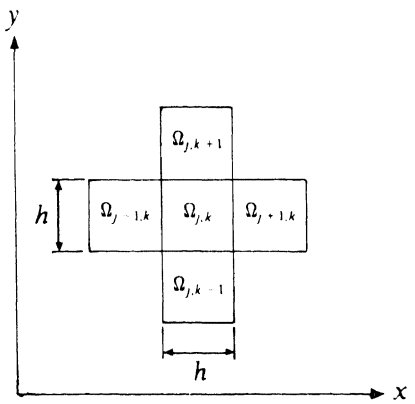

FIG. 2.1. Model volume $\Omega_{j,k}$ with neighbours.

and similar expressions for $u^l_{j-1/2,k}$ and $u^l_{j,k-1/2}$ (the coefficients α_i still free). For the diffusive terms we get

$$\begin{aligned}
\oint_{\partial\Omega_{j,k}} \frac{\partial u}{\partial x} n_x \, ds &= \left[\left(\frac{\partial u}{\partial x}\right)_{j+1/2,k} - \left(\frac{\partial u}{\partial x}\right)_{j-1/2,k}\right] h, \\
\oint_{\partial\Omega_{j,k}} \frac{\partial u}{\partial x} n_y \, ds &= \left[\left(\frac{\partial u}{\partial x}\right)_{j,k+1/2} - \left(\frac{\partial u}{\partial x}\right)_{j,k-1/2}\right] h, \\
\oint_{\partial\Omega_{j,k}} \frac{\partial u}{\partial y} n_y \, ds &= \left[\left(\frac{\partial u}{\partial y}\right)_{j,k+1/2} - \left(\frac{\partial u}{\partial y}\right)_{j,k-1/2}\right] h,
\end{aligned} \tag{2.4a}$$

with

$$\begin{aligned}
\left(\frac{\partial u}{\partial x}\right)_{j+1/2,k} &= \frac{1}{h^2} \oint_{\partial\Omega_{j+1/2,k}} u n_x \, ds = \frac{1}{h}(u_{j+1,k} - u_{j,k}), \\
\left(\frac{\partial u}{\partial x}\right)_{j,k+1/2} &= \frac{1}{h^2} \oint_{\partial\Omega_{j,k+1/2}} u n_x \, ds \\
&= \frac{1}{h}\left[\frac{1}{4}(u_{j,k} + u_{j+1,k} + u_{j,k+1} + u_{j+1,k+1})\right. \\
&\quad \left. - \frac{1}{4}(u_{j-1,k} + u_{j,k} + u_{j-1,k+1} + u_{j,k+1})\right] \\
&= \frac{1}{4h}(u_{j+1,k} + u_{j+1,k+1} - u_{j-1,k} - u_{j-1,k+1}), \\
\left(\frac{\partial u}{\partial y}\right)_{j,k+1/2} &= \frac{1}{h^2} \oint_{\partial\Omega_{j,k+1/2}} u n_y \, ds = \frac{1}{h}(u_{j,k+1} - u_{j,k}),
\end{aligned} \tag{2.4b}$$

and similar expressions for $(\partial u/\partial x)_{j-1/2,k}$, $(\partial u/\partial x)_{j,k-1/2}$, and $(\partial u/\partial y)_{j,k-1/2}$. I (2.4b), $\partial\Omega_{j+1/2,k}$ and $\partial\Omega_{j,k+1/2}$ denote the boundary of shifted volume $\Omega_{j+1/2,k}$ an $\Omega_{j,k+1/2}$, respectively (Fig. 2.2). With the previous flux evaluations we get for eac finite volume $\Omega_{j,k}$ the algebraic equation:

$$\begin{aligned}
&\frac{1}{4}\frac{\varepsilon}{h} u_{j-1,k+1} + \left(\alpha_3 - \frac{\varepsilon}{h}\right) u_{j,k+1} - \frac{1}{4}\frac{\varepsilon}{h} u_{j+1,k+1} \\
&\quad - \alpha_1 u_{j-2,k} + \left(\alpha_1 - \alpha_2 - \frac{\varepsilon}{h}\right) u_{j-1,k} + \left(2\alpha_2 - 2\alpha_3 + 4\frac{\varepsilon}{h}\right) u_{j,k} + \left(\alpha_3 - \frac{\varepsilon}{h}\right) u_{j+1,k} \\
&\quad - \frac{1}{4}\frac{\varepsilon}{h} u_{j-1,k-1} + \left(\alpha_1 - \alpha_2 - \frac{\varepsilon}{h}\right) u_{j,k-1} + \frac{1}{4}\frac{\varepsilon}{h} u_{j+1,k-1} - \alpha_1 u_{j,k-2} = 0,
\end{aligned} \tag{2.}$$

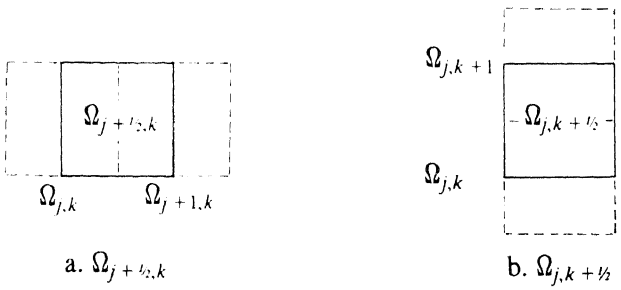

a. $\Omega_{j+1/2,k}$ b. $\Omega_{j,k+1/2}$

FIG. 2.2. Shifted volumes.

with the corresponding stencil:

	$j-2$	$j-1$	j	$j+1$
$k+1$		$\frac{1}{4}\frac{\varepsilon}{h}$	$\alpha_3-\frac{\varepsilon}{h}$	$-\frac{1}{4}\frac{\varepsilon}{h}$
k	$-\alpha_1$	$\alpha_1-\alpha_2-\frac{\varepsilon}{h}$	$2\alpha_2-2\alpha_3+4\frac{\varepsilon}{h}$	$\alpha_3-\frac{\varepsilon}{h}$
$k-1$		$-\frac{1}{4}\frac{\varepsilon}{h}$	$\alpha_1-\alpha_2-\frac{\varepsilon}{h}$	$\frac{1}{4}\frac{\varepsilon}{h}$
$k-2$			$-\alpha_1$	

(2.6)

For point Gauss–Seidel relaxation applied to (2.5), as mentioned before, the four extreme sweep directions are considered (downwind, upwind, and twice crosswind). Introducing n for the number of sweeps performed, these four possibilities can be illustrated as has been done in Fig. 2.3. (In this figure, $u_{j,k}^{n+1}$

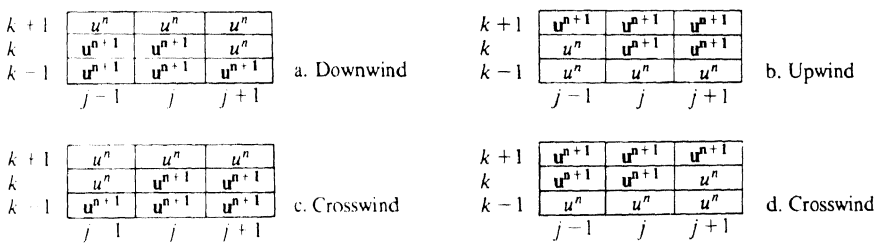

FIG. 2.3. Basic sweep directions, convection direction:

denotes the $(n+1)$th iterate of $u_{j,k}$.) To apply Fourier analysis, we introduce: (i) the iteration error

$$\delta^n_{j,k} = u^*_{j,k} - u^n_{j,k}, \tag{2.7}$$

with $u^*_{j,k}$ the converged numerical solution in $\Omega_{j,k}$ and (ii) the Fourier form

$$\delta^n_{j,k} = D\mu^n e^{i(\omega_1 j + \omega_2 k)h}, \tag{2.8}$$

with D constant, μ the amplification factor, and ω_1 and ω_2 the error frequency in j- and k-directions, respectively. The frequencies to be considered are: $(|\theta_1|, |\theta_2|) \in \{[0, \pi] \times [0, \pi] \mid |\theta_1| \in [\pi/2, \pi] \vee |\theta_2| \in [\pi/2, \pi]\}$, with $\theta_1 \equiv \omega_1 h$, $\theta_2 \equiv \omega_2 h$. Results of the smoothing analysis are given in Section 2.2.

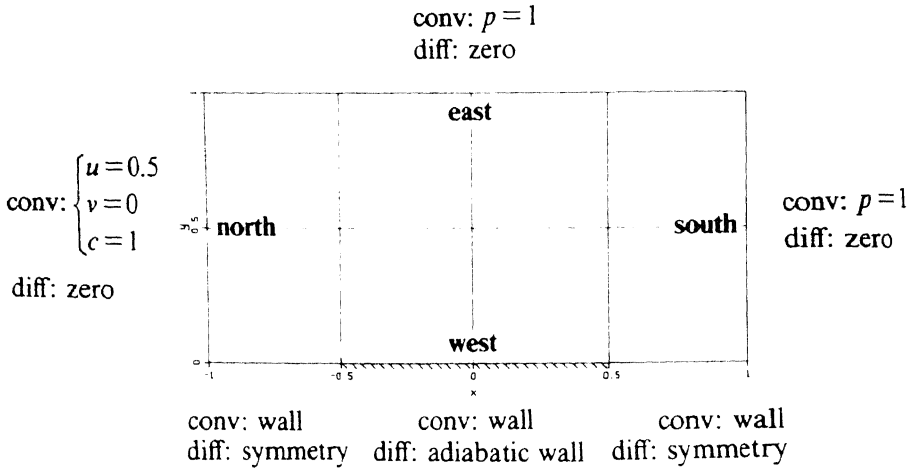

a. Geometry, boundary conditions and coarsest grid (conv: convection, diff: diffusi

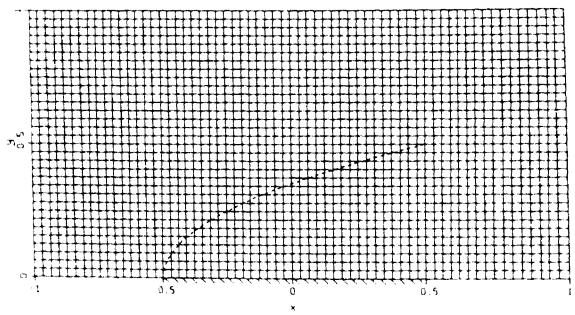

b. Finest grid (------- : boundary layer edge according to Blasius solutio

FIG. 2.4. Subsonic flat plate flow.

2.1.2. *Experiments*

The smooth flow problem considered is a subsonic flat plate flow at $\mathrm{Re} = 100$, for which we can use the Blasius solution [14] as a reference solution. The non-smooth problem considered is a supersonic flat plate flow at $\mathrm{Re} = 2.96 \times 10^5$, with an oblique shock wave impinging upon the flat plate boundary layer and inducing flow separation there. This problem has been taken from [4]. For both flow problems, use is made of: $\gamma = 1.4$ and $\mathrm{Pr} = 0.71$.

The geometry and boundary conditions applied for the subsonic flat plate flow are given in Fig. 2.4a. As far as convection is concerned, the eastern boundary is considered to be an outflow boundary. For diffusion, the northern, southern, and eastern boundary are assumed to be far-field boundaries with zero diffusion. For this subsonic problem we apply grids composed of square finite volumes. The coarsest grid applied in all multigrid computations is the 4×2-grid given in Fig. 2.4a. The finest grid considered is the 64×32-grid given in Fig. 2.4b.

The geometry and boundary conditions for the supersonic flat plate flow are indicated globally in Fig. 2.5a. Here, the coarsest grid is a 5×2-grid (Fig. 2.5a), and

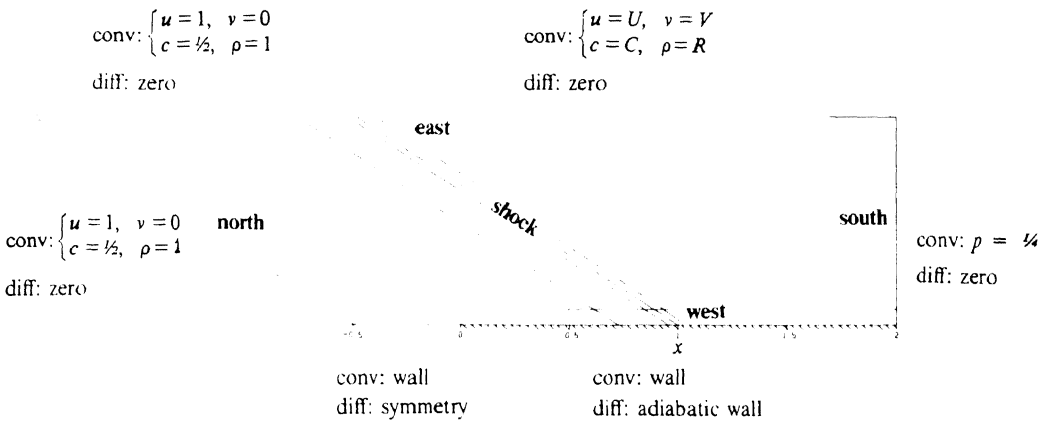

a. Geometry, boundary conditions and coarsest grid (conv: convection, diff: diffusion)

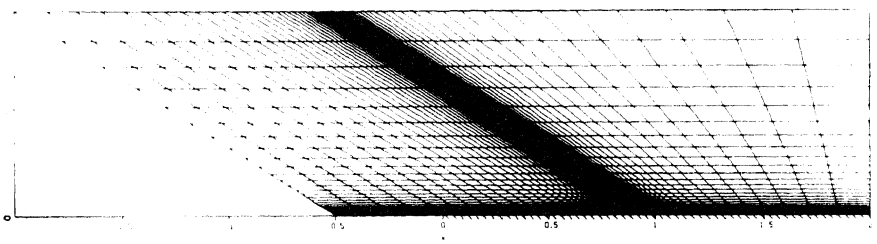

b. Finest grid

FIG. 2.5. Supersonic flat plate flow.

the finest grid a 80×32-grid (Fig. 2.5b). The grids for the supersonic flat plate flow have been optimized for convection by introducing a stretching in j-direction, and in particular by aligning them with the impinging shock wave [8]. The supersonic problem differs essentially from the subsonic problem, both in flow and in grid ((i) non-smooth, supersonic outer flow versus smooth, subsonic outer flow; (ii) thin versus thick boundary layer; (iii) separation, flow reversion, and re-attachment versus none of these; and (iv) non-equidistant, non-orthogonal grid versus equidistant, orthogonal grid.)

For both flow problems, multigrid iteration is applied, using V-cycles with one symmetric pre- and post-relaxation per grid level.

2.2. *Results*

2.2.1. *First-Order Discretized Equations*

For the first-order accurate model discretization we have $\alpha_1 = \alpha_3 = 0$, $\alpha_2 = 1$. With this the general 11-point stencil (2.6) reduces to the following 9-point stencil

	$j-1$	j	$j+1$
$k+1$	$\frac{1}{4}\frac{\varepsilon}{h}$	$-\frac{\varepsilon}{h}$	$-\frac{1}{4}\frac{\varepsilon}{h}$
k	$-\left(1+\frac{\varepsilon}{h}\right)$	$2+4\frac{\varepsilon}{h}$	$-\frac{\varepsilon}{h}$
$k-1$	$-\frac{1}{4}\frac{\varepsilon}{h}$	$-\left(1+\frac{\varepsilon}{h}\right)$	$\frac{1}{4}\frac{\varepsilon}{h}$

(2.9)

Using the iteration error (2.8) we obtain the smoothing results given in Fig. 2.6. In Fig. 2.6a, for each of the four possible sweep directions, the smoothing factor $\mu_s = \sup|\mu(\theta_1, \theta_2)|$ is given as a function of ε/h. In Fig. 2.6b, for $\varepsilon/h = 1$, the corresponding distributions $|\mu(\theta_1, \theta_2)|$ are given. (All four distributions are point-symmetric with respect to $\theta_1 = 0$, $\theta_2 = 0$.) Clearly visible in Fig. 2.6a is the good smoothing for any value of ε/h and any convection direction, when sweeping alternatingly in all four different directions (for instance, by applying symmetric sweeps and by using a different diagonal sweep direction in pre- and post-relaxation).

For the subsonic flat plat flow, the multigrid method's behaviour is illustrated in Fig. 2.7 by a graph of the residual ratio $\sum_{i=1}^{4} |(F_h(q_h^n))_i| / \sum_{i=1}^{4} |(F_h(q_h^0))_i|$ versus the number of cycles performed. Here, $|(F_h(q_h^n))_i|$ denotes the summation—over all finest grid volumes—of the absolute values of the ith component in the first-order Navier–Stokes defects, with q_h^n the nth iterate and q_h^0 the approximate solution obtained by the nested iteration [6]. The measure of grid-independence of the multigrid method is illustrated by convergence histories obtained on a 16×8-, a 32×16-, and a 64×32-grid. For the flow considered, the method appears to be

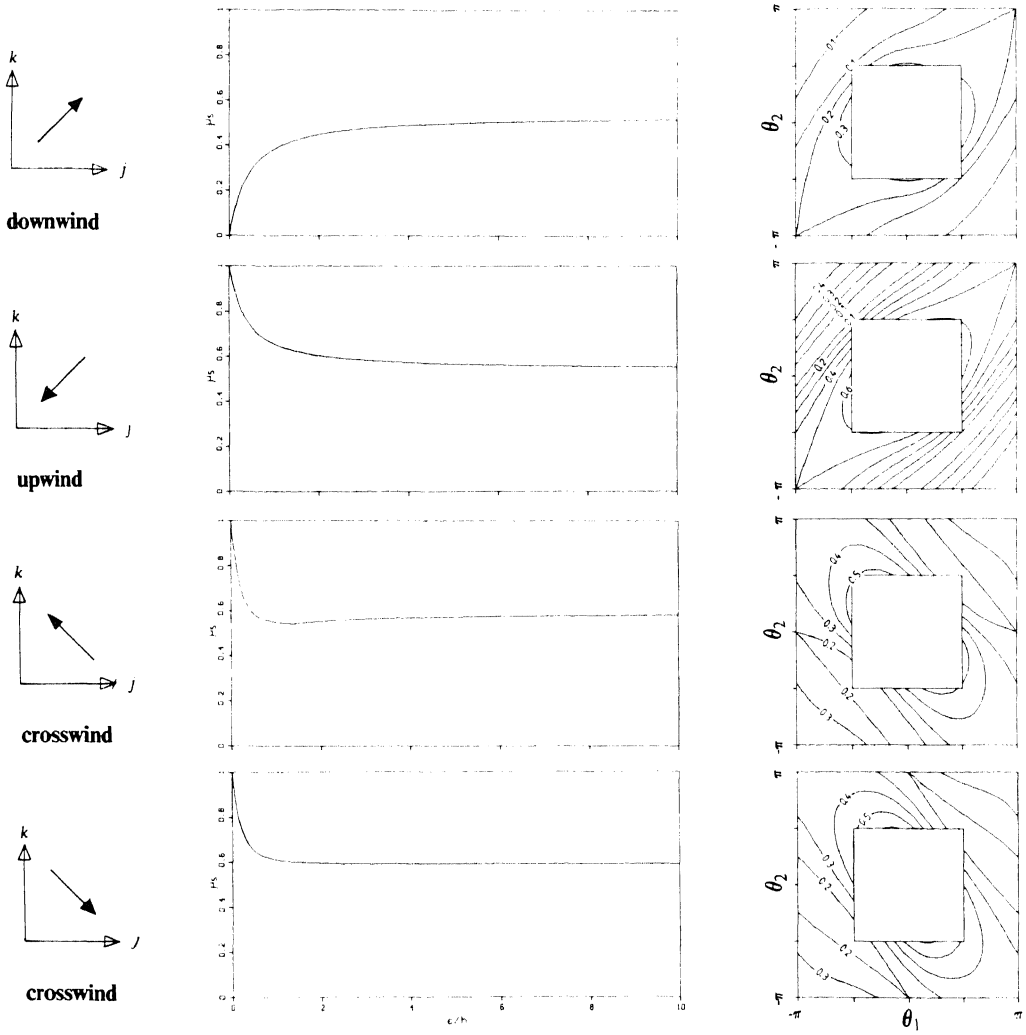

a. Versus ϵ/h b. For $\epsilon/h = 1$

FIG. 2.6. Smoothing factors point Gauss–Seidel relaxation, first-order discretized model equation.

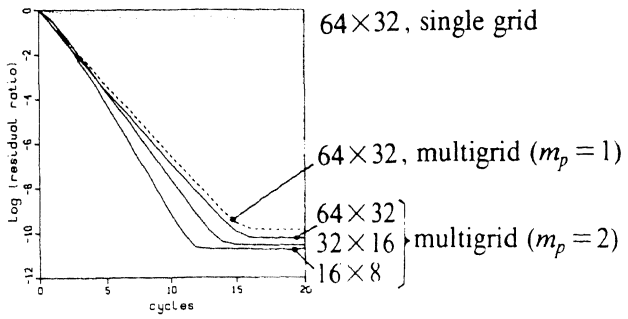

FIG. 2.7. Multigrid behaviour for the subsonic flat plate flow, first-order discretized Navier–Stokes equations.

nearly grid-independent. In the same figure, the multigrid effectiveness is illustrated by giving the convergence history for a single-grid computation on the 64×32-grid, with one (single-grid) cycle being defined as a symmetric relaxation sweep. Further, in the same figure, the influence of the higher-order accuracy of the correction prolongation is illustrated by also giving the convergence history for a multigrid strategy with $m_p = 1$ (so violating the rule $m_p + m_r > 2m$ [3]). Already for this moderately convection dominated flow ($\mathrm{Re} = 100$), the positive influence of the second-order prolongation appears to be negligible. Using the Blasius solution as a reference, in Fig. 2.8 it is shown that only a single FAS-cycle is sufficient for converging to discretization error accuracy. (In Fig. 2.8c, the multigrid effectiveness is illustrated once more by giving single-grid results.)

For the supersonic flat plate flow, similar convergence results are shown in Figs. 2.9 and 2.10 for a 20×8-, a 40×16-, and a 80×32-grid. Here we used the first-order prolongation only. The deterioration of the multigrid method's convergence behaviour for the 80×32-grid case, as most clearly visible in Fig. 2.10c, is probably

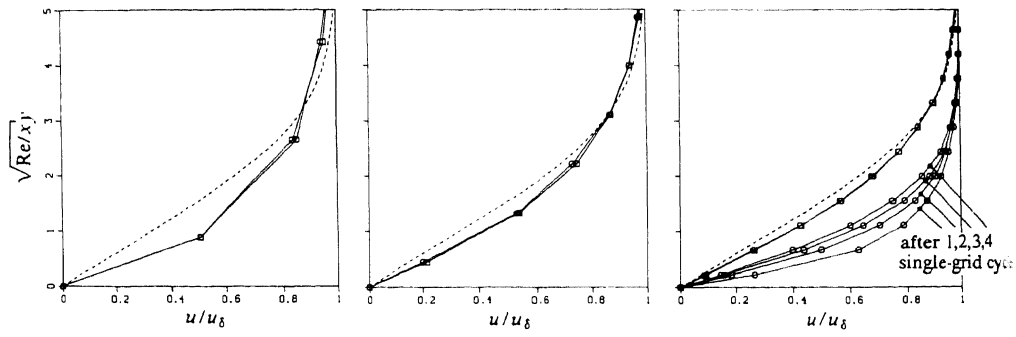

a. On 16×8-grid b. On 32×16-grid c. On 64×32-grid

FIG. 2.8. Velocity profiles at $x = 0$ for the subsonic flat plate flow, first-order discretized Navier–Stokes equations (----: Blasius solution, ○: after 1 FAS-cycle, □: after 20 FAS-cycles).

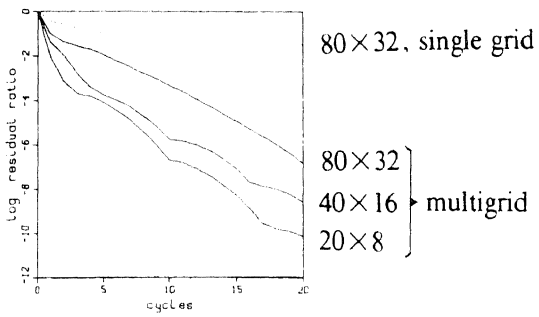

FIG. 2.9. Multigrid behaviour for the supersonic flat plate flow, first-order discretized Navier-Stokes equations.

due to essential differences between this fine grid solution and the underlying coarser grid solutions. If desired, application of sophisticated grid transfer operators might be efficacious for matching the smooth problem's convergence rates. (Throughout the complete domain, the solution prolongation in the nested iteration is simply bilinear, and the correction prolongation in the nonlinear multigrid iteration is simply piecewise constant. Just as with the Euler equations, restriction of the solution is even omitted; we simply take the latest solution obtained.) Despite the deterioration with respect to the subsonic flat plate flow, the multigrid method's performance for this problem is already competitive with two well-established solution methods for the full Navier–Stokes equations: those of Beam and Warming [1] and MacCormack [11]. Using a CDC 7600, Beam and Warming and MacCormack convergence to steady state for 32×32- and 32×45-grids, respectively, in 100 and 256 iterations, and 46 and 40 ms per grid point, respectively. Using a (single-pipe) CDC Cyber 205, with the present multigrid method we need for the 80×32-grid: 5 iterations (FAS-cycles) and 23 ms per finite volume, without

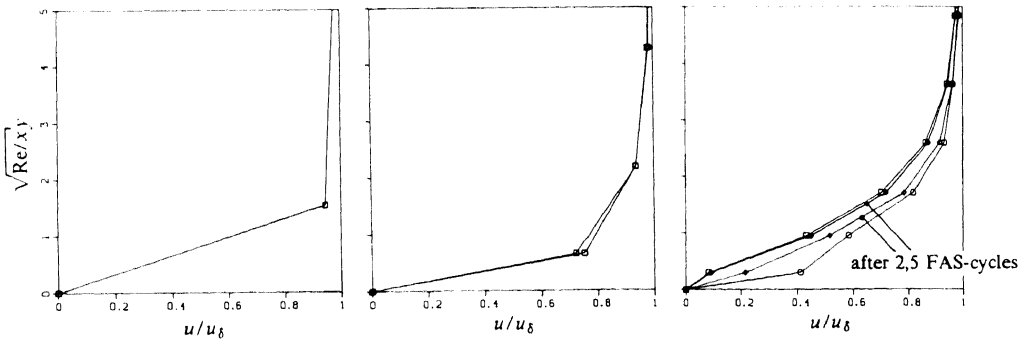

a. On 20×8-grid b. On 40×16-grid c. On 80×32-grid

FIG. 2.10. Velocity profiles at $x = 1$ for the supersonic flat plate flow, first-order discretized Navier–Stokes equations (○: after 1 FAS-cycle, ||: after 20 FAS-cycles).

optimization for vectorization. Though the Beam-Warming and MacCormack methods are supposed to be somewhat more prone to vectorization, for finer and finer discretizations, the present multigrid method will be more and more efficient than these methods, due to its better grid-independence. Yet, the main advantage of the present method lies in the significantly smaller number of iterations required. For large-scale computations for which all data cannot be kept in core, a small number of iterations required results in a small number of out-of-core data transports. Since, in particular, for large-scale Navier–Stokes flow computations, IO-times rather than CPU-times may be the hampering factor, this property is an important advantage of the present multigrid method. In relation to this, it should be emphasized that though the present method is fully implicit, it imposes very mild computer memory requirements due to the fact that the relaxation is only point-wise. (No large matrices are stored.)

2.2.2. *Second-Order Discretized Equations*

For the second-order accurate model discretization we have $\alpha_1 = -\frac{1}{6}$, $\alpha_2 = \frac{5}{6}$, $\alpha_3 = \frac{1}{3}$. With these values, (2.6) becomes

	$j-2$	$j-1$	j	$j+1$
$k+1$		$\frac{1}{4}\frac{\varepsilon}{h}$	$\frac{1}{3}-\frac{\varepsilon}{h}$	$-\frac{1}{4}\frac{\varepsilon}{h}$
k	$\frac{1}{6}$	$-\left(1+\frac{\varepsilon}{h}\right)$	$1+4\frac{\varepsilon}{h}$	$\frac{1}{3}-\frac{\varepsilon}{h}$
$k-1$		$-\frac{1}{4}\frac{\varepsilon}{h}$	$-\left(1+\frac{\varepsilon}{h}\right)$	$\frac{1}{4}\frac{\varepsilon}{h}$
$k-2$			$\frac{1}{6}$	

(2.10)

For the four extreme sweep directions, this yields the smoothing results given in Fig. 2.11. Only for $\varepsilon/h > 1$ there is some acceptable smoothing. For problems which are locally convection dominated, the present smoothing factors are unacceptable, except for those belonging to the purely downwind sweep. Since purely downwind relaxation sweeps are not feasible in practice and since no specific alternation of sweep directions is supposed to suffice, another remedy has to be found. A standard method would be to explicitly add some artificial diffusion, to ensure diagonal dominance. But, of course, adding artificial diffusion reduces the accuracy. Further, adding the proper amount of diffusion may require much trial and error. Since we want to avoid both, we solve the unimpaired system of higher-order discretized equations by iterative defect correction. This implies the repeated solution of some lower-order system with diagonal dominance guaranteed, with the higher-order

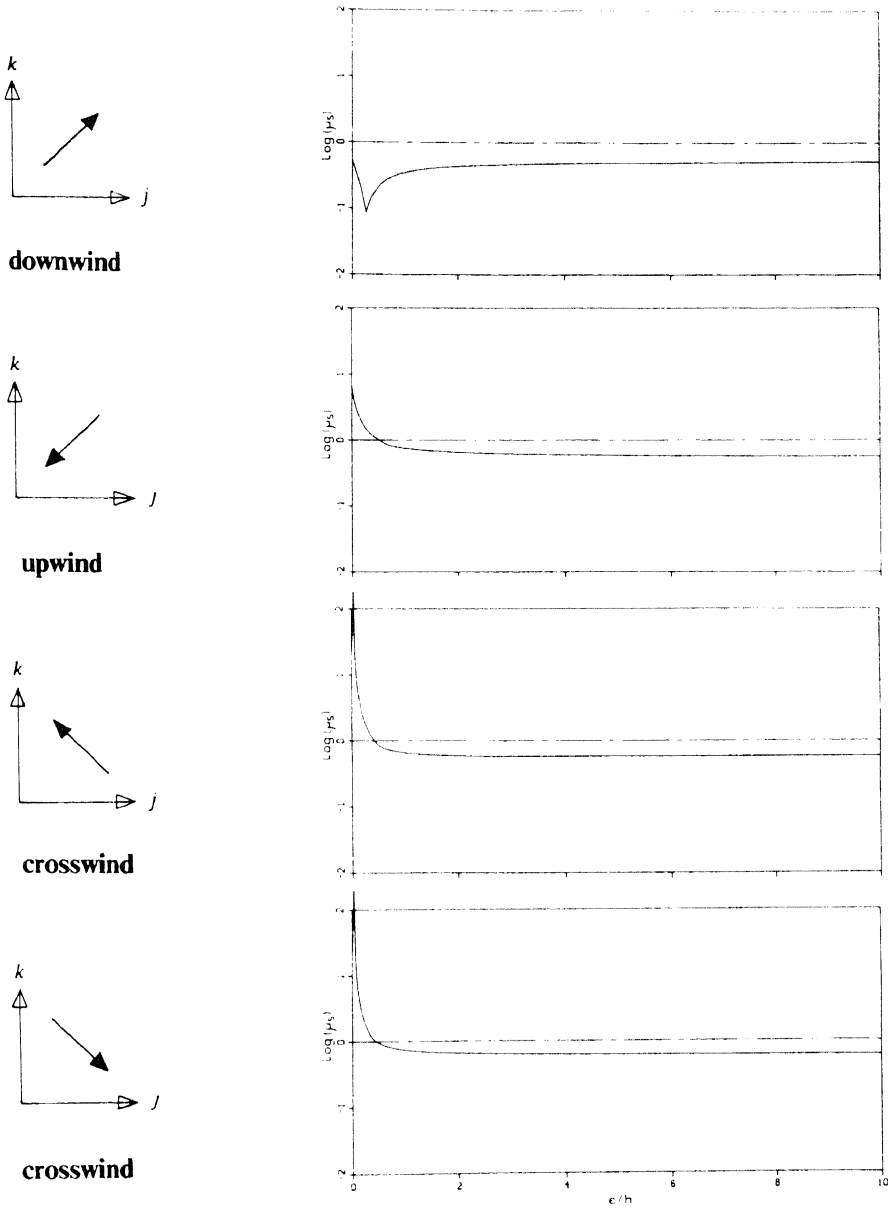

FIG. 2.11. Smoothing factors point Gauss–Seidel relaxation, second-order discretized model equation.

target operator working via the right-hand side. This approach has already proved to be successful for the steady Euler equations [7]. For the steady Navier–Stokes equations now, the big difference with the Euler equations in applying iterative defect correction is the much greater freedom in the choice of the lower-order operator to be inverted, a freedom that may be exploited. Making a favourable choice for this operator is the main topic of Section 3.

Though iterative defect correction is well-developed as far as it concerns the mathematical concept [2, 3], it is underdeveloped as far as it concerns applications. The present application to the steady Navier–Stokes equations, for instance, is a novelty. An important property of iterative defect correction is that it allows convergence to second-order accuracy in only one iteration [3]. Given the availability of efficient inner solution method(s), the efficiency of a method with defect correction as outer iteration may be hard to beat.

3. Convergence of Iterative Defect Correction

The iterative defect correction (IDeC-) method can be written as

$$\begin{aligned} &\tilde{F}_h(q_h^0) = 0, \\ &\tilde{F}_h(q_h^{n+1}) = \tilde{F}_h(q_h^n) - \omega F_h(q_h^n), \qquad n = 0, 1, \ldots, N, \end{aligned} \tag{3.1}$$

with the superscript n denoting the iteration counter and ω a possible damping factor. (The standard value for ω is $\omega = 1$.) The discrete operators considered are (i) the higher-order accurate target operator F_h which for the model equation is defined by (2.10) and (ii) the approximate operator $\tilde{F}_h$, the operator to be inverted A requirement to be fulfilled by $\tilde{F}_h$, as seen in Section 2.2.2, is that it must have a first-order accurate convective part. The choice of the diffusive part is still free Two, in this sense, extreme possibilities are already available: (i) the operato without diffusive terms as used for the Euler equations [7] and (ii) the operato with second-order accurate diffusion as considered in Section 2.2.1. The advantag of the first approximate operator is its greater simplicity. For the second operato this is its closer resemblance to the target operator F_h. It complies with the theor that for sufficiently smooth problems, the solution will be second-order accurat after a single IDeC-cycle only. As an intermediate alternative we also consider th approximate operator which neglects mixed derivatives. This operator combines, i some intermediate way, simplicity and good resemblance.

As in Section 2, both theoretical and experimental results are presented. Th theoretical results are obtained by Fourier analysis for the same model equatio as in Section 2. (The analysis is made for both the outer and inner iteratio convergence and smoothing analysis, respectively.) The experimental results a obtained for the same two flow problems as in Section 2.

3.1. *Theoretical Results*

Concisely written, the three approximate operators to be considered are: (i) the first-order accurate convection operator

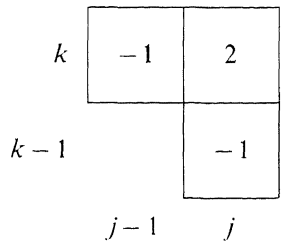

(3.2)

(ii) the zeroth-order accurate convection-diffusion operator

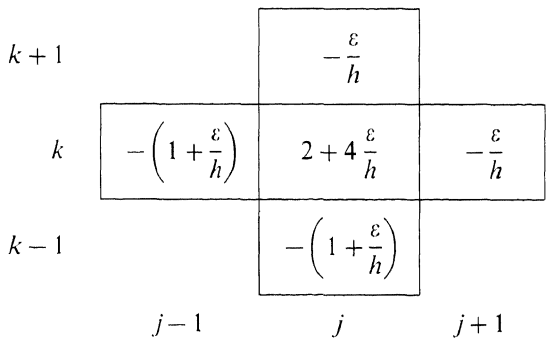

(3.3)

(iii) the first-order accurate convection-diffusion operator (2.9).

For the model equation (2.1), iteration (3.1) is rewritten as

$$\begin{aligned} &\tilde{F}_h(u_h^0) = 0, \\ &\tilde{F}_h(u_h^{n+1}) = (\tilde{F}_h - \omega F_h)(u_h^n), \qquad n = 0, 1, ..., N. \end{aligned} \tag{3.4}$$

Introducing as before the iteration error (2.7) in its Fourier form (2.8), we can write for the convergence factor μ:

$$\mu(\theta_1, \theta_2) = 1 - \omega \tilde{F}_h^{-1}(\theta_1, \theta_2)\, F_h(\theta_1, \theta_2). \tag{3.5}$$

For $\omega = 1$, convergence results are given in Fig. 3.1. In Fig. 3.1a, for each of the three approximate operators (3.2), (3.3), and (2.9), the convergence factor $\mu_c = \sup|\mu(\theta_1, \theta_2)|$, $\omega = 1$, $(|\theta_1|, |\theta_2|) \in \{[0, \pi] \times [0, \pi]\}$ is given as a function of ε/h. In Fig. 3.1b, for $\varepsilon/h = 4/9$, $\varepsilon/h = 1$, and $\varepsilon/h = \infty$, the corresponding distributions of $|\mu(\theta_1, \theta_2)|$ are given. From Fig. 3.1a it appears that for small values of ε/h, the approximate operator (3.2) yields the best convergence rate. However, as was to be expected, for increasing ε/h its convergence starts to deteriorate (from $\varepsilon/h = 4/9$)

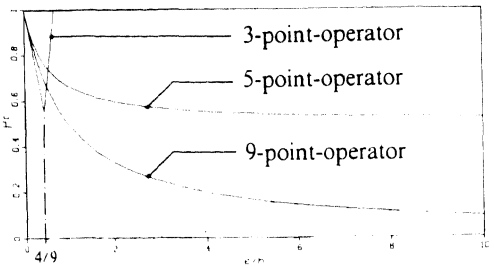

a. Versus ϵ/h

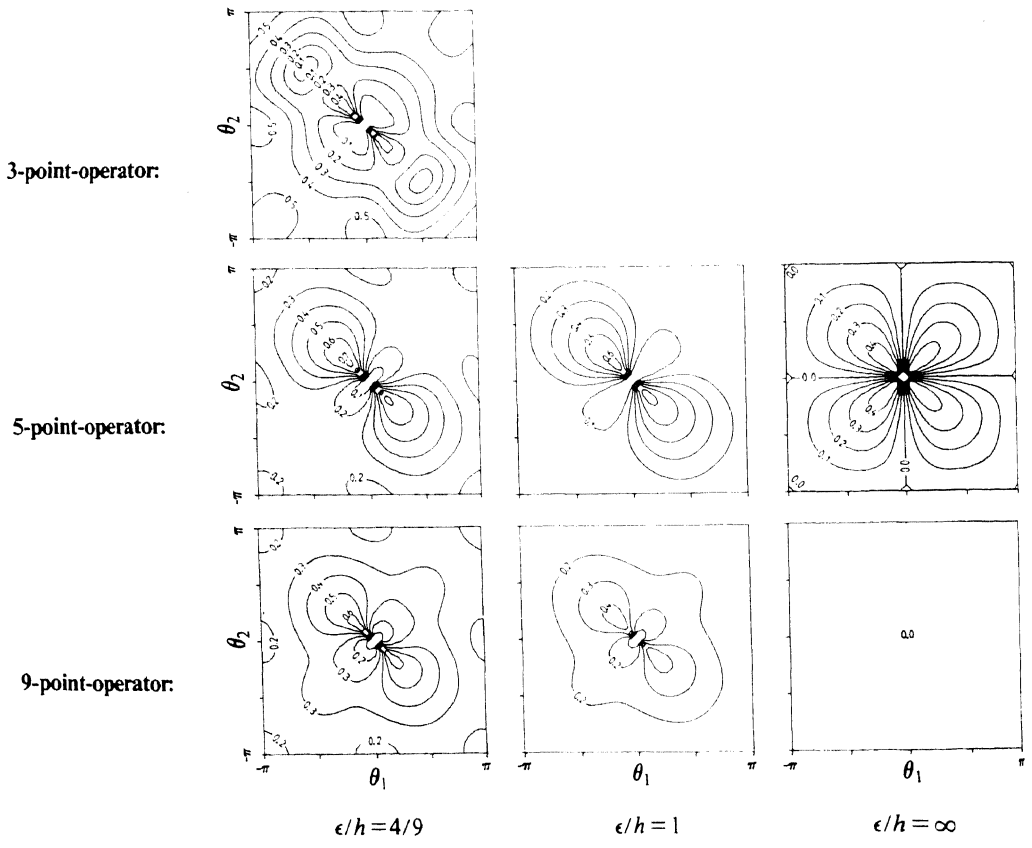

b. For $\epsilon/h = 4/9$, $\epsilon/h = 1$ and $\epsilon/h = \infty$

FIG. 3.1. Convergence factors iterative defect correction, second-order discretized model equation.

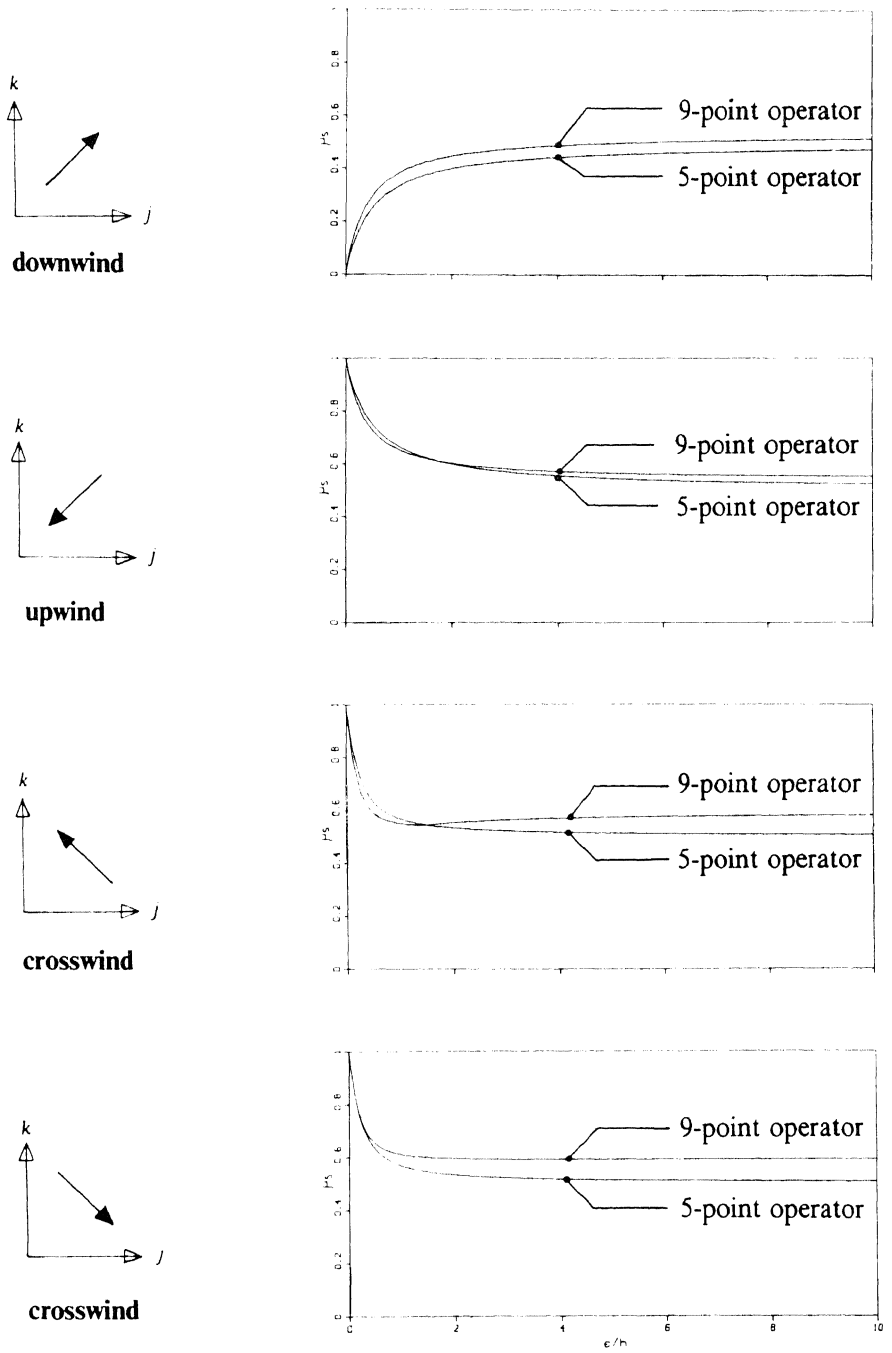

FIG. 3.2. Smoothing factors point Gauss–Seidel relaxation, zeroth- and first-order discretized model equation.

and finally turns into divergence (at $\varepsilon/h = 2/3$). Even for high-Reynolds number flows, local regions with diffusion dominating convection may arise. Therefore, approximate operator (3.2) has to be rejected. As far as the convergence rate of the two remaining operators is concerned, the 9-point operator (2.9) clearly is to be preferred above the 5-point alternative (3.3).

However, the 5-pointer might behave better in the inner iteration (point Gauss–Seidel accelerated by multigrid). In Fig. 3.2, for the four extreme sweep directions, its smoothing factors μ_s are given as a function of ε/h. For comparison, the smoothing factors for the 9-point operator (Fig. 2.6) have been added. It appears that both operators nearly have the same good smoothing behaviour, the 5-pointer being only slightly better. Because of its superior behaviour in IDeC (Fig. 3.1), we prefer the 9-pointer as operator to be inverted. (Its relative complexity is taken for granted.)

3.2. *Experimental Results*

For the subsonic flat plate flow, results are shown in Fig. 3.3. Given for the 16×8-, 32×16-, and 64×32-grid is the velocity profile obtained on the middle of the plate after 1 IDeC-cycle and 50 IDeC-cycles (full convergence). In all cases we performed a single FAS-cycle per IDeC-cycle only. In agreement with theory [3], only a single IDeC-cycle appears to be sufficient for obtaining second-order accuracy.

In the same way, for the supersonic flat plate flow we also show velocity profiles on three successive grids (Fig. 3.4). Per IDeC-cycle we apply again one FAS-cycle. The velocity profile considered is that at $x = 1$ (where the shock wave impinges the plate in case of inviscid flow). As was to be expected, here we also observe some deterioration of the convergence rate for the 80×32-grid case. For this case, fo

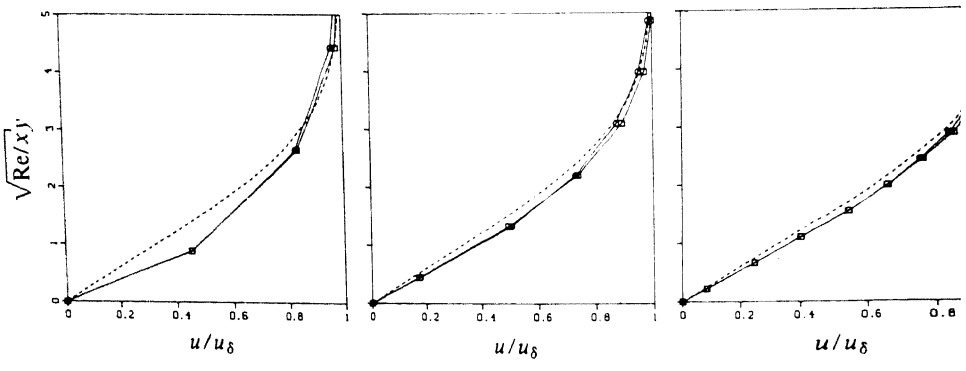

a. On 16×8-grid b. On 32×16-grid c. On 64×32-grid

FIG. 3.3. Velocity profiles at $x = 0$ for the subsonic flat plate flow (non-limited) second-order discretized Navier–Stokes equations (○: after 1 IDeC-cycle, ▯: after 50 IDeC-cycles).

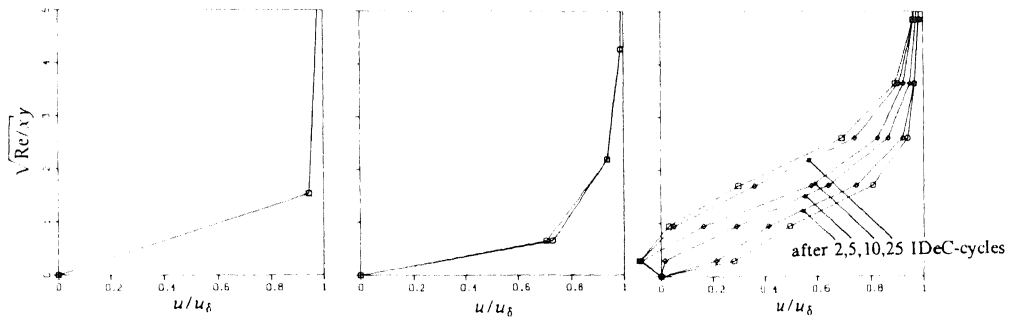

a. On 20×8-grid b. On 40×16-grid c. On 80×32-grid

FIG. 3.4. Velocity profiles at $x = 1$ for the supersonic flat plate flow, (limited) second-order discretized Navier–Stokes equations (○: after 1 IDeC-cycle, □: after 50 IDeC-cycles).

which we also give the velocity profile as obtained after 2, 5, 10, and 25 IDeC-cycles (Fig. 3.4c), we had to use the limiter and to take $\omega = \frac{1}{2}$.

4. CONCLUSIONS

For the computation of *smooth* flow problems with the steady Navier–Stokes equations, nonlinear multigrid and iterative defect correction appear to be very efficient tools. For these problems, the ultimate multigrid goal, convergence in a few work units only, is attained for both the first- and second-order discretized equations; the latter without introduction of anything artificial. It appears that even for moderately convection dominated ($\mathrm{Re} = O(10^2)$) smooth flow problems, it is not necessary to satisfy the multigrid rule which requires the sum of order of prolongation and restriction to exceed the order of the Navier–Stokes equations. The most essential element for the success of the multigrid technique is the collective symmetric point Gauss–Seidel relaxation with inside that: exact Newton iteration applied to the continuously differentiable, first-order discretized, full Navier–Stokes equations. The most essential element for the success of the iterative defect correction technique is the first-order upwind Navier–Stokes operator as the approximate operator. An additional advantage of the present method, as it stands for smooth flow problems, is that it is completely parameter-free; it needs no tuning of parameters.

For *non-smooth* problems the convergence properties are not yet as good as those for smooth problems, though already competitive with those of well-established methods.

A general advantage of the method is that, though it is fully implicit, it imposes very low computer memory requirements.

ACKNOWLEDGMENTS

The author wants to thank Professor Hemker and Professor Wesseling for their constructive comments.

REFERENCES

1. R. M. BEAM AND R. F. WARMING, *AIAA J.* **16**, 393 (1978).
2. K. BÖHMER, P. W. HEMKER, AND H. J. STETTER, *Comput. Suppl.* **5**, 1 (1984).
3. W. HACKBUSCH, *Multi-Grid Methods and Applications* (Springer-Verlag, Berlin, 1985).
4. R. J. HAKKINEN, I. GREBER, L. TRILLING, AND S. S. ABARBANEL, NASA-memorandum 2-18-59 W, 1959 (unpublished).
5. P. W. HEMKER AND S. P. SPEKREIJSE, *Appl. Numer. Math.* **2**, 475 (1986).
6. B. KOREN, *Int. J. Numer. Methods in Fluids* **9**, 59 (1989).
7. B. KOREN, *J. Comput. Phys.* **77**, 183 (1988).
8. B. KOREN, in *Notes on Numerical Fluid Mechanics*, Vol. 24, edited by J. Ballmann and R. Jeltsch (Vieweg, Braunschweig, 1989).
9. B. VAN LEER, in *Lecture Notes in Physics*, Vol. 170, edited by E. Krause (Springer-Verlag, Berlin, 1982).
10. B. VAN LEER, in *Lectures in Applied Mathematics*, Vol. 22, edited by B. E. Engquist *et al.* (Amer. Math. Soc., Providence, RI, 1985).
11. R. W. MACCORMACK, *AIAA J.* **20**, 1275 (1982).
12. S. OSHER AND F. SOLOMON, *Math. Comput.* **38**, 339 (1982).
13. R. PEYRET AND T. D. TAYLOR, *Computational Methods for Fluid Flow* (Springer-Verlag, Berlin, 1983).
14. H. SCHLICHTING, *Boundary-Layer Theory* (McGraw-Hill, New York, 1979).
15. S. P. SPEKREIJSE, *Math. Comput.* **49**, 135 (1987).